Online Supplemental Data

Supplemental Methods

Rabbit monoclonal antibody against Nox4

Nox4 antibody was raised against a peptide sequence within the NADPH binding domain of Nox4 that is unique to human and mouse NADPH oxidase sequences (the sequence is conserved between human and mouse Nox4 proteins). The antibodies were generated in collaboration with and are now available through Epitomics (Burlingame, Calif). Hybridoma clones were generated from B cells from one of the immunized rabbits and screened. Protein-G Sepharose-purified monoclonal antibodies were used to perform Western blotting, immune-precipitation and immunohistochemistry experiments.[1, 2] The other antibodies used in this study are listed in Supplemental Table S2.

Generation and identification of cardiac-specific human Nox4 transgenic (c-hNox4Tg) mice

The Cre-lox system was used to generate the c-hNox4Tg mice. Lox-Stop-lox-human Nox4 transgenic mice (LSL-hNox4Tg) on a mixed genetic background of 129 and C57BL/6 were created in collaboration with Taconic Farm, Inc. In these transgenic mice, the transgene construct contains loxP-flanked DNA STOP sequence, driven by a beta-actin promoter, preventing expression of the downstream hNox4 (human Nox4) gene. When the LSL-hNox4Tg mice are crossed with alpha-MHC-MerCreMer transgenic mice (Jackson Laboratory, Stock #005650), the tamoxifen-inducible Cre-mediated recombination is expected to result in deletion of the floxed STOP sequence leading to expression of hNox4 specifically in myocardium of the offspring (Supplemental Figure S1A).

Tail tissue of the offspring were harvested and the polymerase chain reaction (PCR) assays were performed to identify c-hNox4 Tg pups using the following primers: αMHC-Cre forward 5'-AGG TGG ACC TGA TCA TGG AG-3', αMHC-Cre reverse 5'- ATA CCG GAG ATC ATG CAA GC-3'; LSL forward CGG ATC CTC GGG GAC ACC AAA TAT G, LSL reverse AAG GCA TTC CAC CAC TGC TCC C; hNox4 forward 5'-ACC TTT GTG CCT GTA CTG TGC C-3', hNox4 reverse 5'-TGT TGC TTT GGT TTC AGT TGG AC-3'; Mouse Nox4 forward 5'-TCC AAG CTC ATT TCC CAC AGA CC-3', mouse Nox4 reverse 5'-GTG GAC ACC AAA TGT TGC T-3'. Reverse transcription polymerase chain reaction (RT-PCR) assays were carried out to identify the expression of transgenic hNox4 in myocardium and liver (Figure 1A and 1B).

Blood pressure measurement

Blood pressure of mice was measured using The CODA 8-Channel High Throughput Non-Invasive Blood Pressure system (Kent Scientific Co.). Measurements were made on conscious mice. Systolic and diastolic blood pressure, heart rate, mean blood pressure, tail blood flow, and tail blood volume were recorded.

Immunoblot analysis

Homogenates of left ventricle tissue were prepared in RIPA lysis buffer containing 20 mM Tris·HCl, pH 7.5, 150 mM NaCl, 5 mM EDTA, 1 mM Na3VO4, 1 mM PMSF, 20 µg/ml aprotinin, 20 µg/ml leupeptin, 1% NP-40. Protein concentrations of samples were determined by the Bio-Rad protein assay. Samples were subjected to SDS-PAGE. Proteins were transferred onto polyvinylidene fluoride microporous membranes (Bio-Rad). The membranes were blocked with 5% low-fat milk in Tris-buffered saline and then probed with primary antibodies (1:1000 dilution). The primary antibodies used in this study included antibodies against Nox4 (monoclonal

antibody from Epitomics or polyclonal antibody from Santa Cruz), Mox1 (Abcam), alpha-SM-actin (Abcam), and the remaining antibodies were purchased from Cell Signaling Tech. The appropriate HRP-conjugated secondary antibodies were added (1:3000) and bands were visualized by enhanced chemiluminescence. Densitometric analysis was performed using NIH Image/ImageJ software.[3]

Quantitative real-time reverse transcription polymerase chain assay (qPCR)

The assay of qPCR was performed to quantify expression of the following genes: mouse Nox isoforms 1 to 4 and transgenic hNox4, transforming growth factor beta (TGF-β), collagen-1 alpha 1, collagen-3 alpha 1, connective tissue growth factor (CTGF), plasminogen activator inhibitor-1 (PAI-1). GAPDH was used as the internal control. Sequences of primers used in this study were summarized in Supplemental Table S3. SYBR green I dye method was used for qPCR assay. In brief, after preparing total RNA, first-strand cDNA was synthesized by reverse transcription. Real-time PCR was conducted on a 7500 Fast Real-Time PCR System (Applied Biosystems) using the Power SYBR® Green Master Mix (Applied Biosystems). Comparative Ct (ΔΔCt) method was utilized to rapidly and accurately calculate relative gene expression across all the tests.

Dihydroethidium staining

Dihydroethidium (DHE), relatively specific for superoxide anion measurement, is an oxidative fluorescent dye that undergoes a two-electron oxidation to form the DNA-binding fluorophore ethidium bromide. The DHE (Calbiochem, Darmstadt, Germany) staining for superoxide was carried out as previously described.[3, 4] Briefly, unfixed left ventricular frozen samples were cut into 10-μm-thick sections and placed on glass slides. DHE (10 μmol/l) was applied to each tissue section, and the slides were incubated in a light-protected humidified chamber at 37°C for 15 min. Fluorescent images of ethidium-stained tissue were obtained with a laser-scanning confocal microscope (Zeiss 510 NLO). Ethidium bromide was excited at 488 nm, and fluorescence was detected at 560 nm long-pass filter. Mean fluorescence intensity of the digitized image was measured with ImageJ software [version 1.35, National Institutes of Health (NIH), Bethesda, MD] for quantification. Generation of superoxide was demonstrated by red fluorescent labeling. Nonstained left ventricular sections were used as background control. The average of five sections stained with DHE was taken as the value for each animal. Ethidium fluorescence (excitation at 490 nm, emission at 610 nm) was examined by fluorescent microscopy.

Hydrogen peroxide assay

Intracellular hydrogen peroxide was evaluated using a genetically encoded fluorescent sensor-HyPer (Cat # FP941, Evrogen). In brief, freshly frozen sections of the left ventricles were transfected with pHyPer-cyto vector using Optifect transfection reagent. 24 hrs post transfection incubation, the green fluorescence (530/30 nm bandpass filter) in transfected sections after excitation at 488 and 405 nm was measured using a BD FACSAria II SORP flow cytometer. The production of intracellular H_2O_2 was measured by calculating the ratio of green fluorescence excited at 488 and 405 nm.

Detection of apoptosis

To detect apoptosis of cardiomyocytes of LV, TUNEL staining was conducted as described before.[5] TUNEL staining using the TUNEL Apoptosis Detection Kit (Upstate) was performed according to the manufacturer's instructions. The sections were examined using light microscopy. Sections incubated with PBS, instead of TDT enzyme solution, served as the negative controls. The number of TUNEL-positive cells was counted in five randomly selected fields under 400x magnification for each animal. Four animals were studied per group.

Masson's trichrome staining

Masson's trichrome is a three-color staining assay used to recognize collagen composition of tissues in histology. Masson's trichrome staining was performed as previously described.[6, 7] Frozen sections embedded in OCT compound were used in this study. Cryosections were first fixed in 4% paraformaldehyde for 1 hour and then re-fixed in Bouin's solution overnight at room temperature. The collagen fibers were stained blue and the nuclei stained black and cytosol stained red.

Heamatoxylin-Eosin staining

Heamatoxylin-Eosin (HE) staining method, involves application of hemalum, which is a complex formed from aluminum ions and oxidized haematoxylin. This colors nuclei of cells (and a few other objects, such as keratohyalin granules) blue. The nuclear staining was followed by counterstaining with an aqueous or alcoholic solution of eosin, which colors other, eosinophilic structures in various shades of red, pink and orange.

Quantitative morphometric analysis

At sacrifice, the mice were perfused with 1XPBS containing potassium chloride to arrest the hearts in diastole. Morphometric analyses were carried out to relatively quantify myocyte size, interstitial fibrotic area, number of apoptotic cells, and intensity of DHE staining in cross-sections of LV tissues chemically stained by the protocols described above. Each LV was cross-sectionally cut into three parts, apex, the middle portion and the bottom. The bottom and apex parts were saved at – 80°C for analyses of protein and mRNA expression. The middle portions were embed in OCT compound and saved at – 80°C. Three serial cross-cryosections of the middle portion at a 300-µm-interval were used for the morphological analyses. Images of 16 fields (views with 400x magnification) of each cross-section along each of 8 radial lines (2 fields on each radial line) were visualized, captured under a microscope Zeiss Fluorescent Axio Scope-A1with an AxioCam MRc5 camera. The 48 images of one LV were used to manually count apoptotic cells (20 cells in each field were counted), or quantify cell size and fibrotic area by using Image-Pro software. Using Image Pro and after calibration with a stage micrometer, the areas of interests can be circled by tracing the edge of the interested target and the values of quantified areas were exported to a spreadsheet in square micrometers. This is repeated for each image of LV tissue section. One mean value of cell sizes or fibrotic areas averaged from 16 images was averaged for one section. All the measurements (total 48) of 3 serial sections of a LV were averaged into a mean value representing the result for one mouse (Supplemental Figure S2).

NADPH oxidase assay

NADPH oxidase activity was measured by the lucigenin-enhanced chemiluminescence method. Left ventricles of the mouse hearts (a small piece) were homogenized in 400 µl of ice-cold lysis buffer (20 mM KHPO4, pH 7.0) containing a mixture of protease inhibitors using ultrasonic cell disruptor tissue homogenates were allowed to stand for 10 min. on ice. Total protein content was measured using the Bio-Rad protein assay reagent. To start the assay, 150 µg of total protein from each homogenate were added to assay buffer (50 mM phosphate buffer, pH 7.0, containing 1 mM EGTA and 150 mM sucrose), 5 µM lucigenin, and 100 µM NADPH in 500ul of reaction. Photon emission in terms of relative light units was measured every 30 sec. for 5 min. using a luminometer. Superoxide production was expressed as relative chemiluminescence (light) units/min/mg of protein.

Tissue explant culture of left ventricle and treatments

Under sterile conditions, Tg mice infused with AngII (Tg+AngII) were decapitated and hearts were excised. The hearts were rinsed 3 times in cold Hank's balanced salt solution containing 2× strength antibiotics (200 U/mL of penicillin, 200 µg/mL of streptomycin). Atria and right ventricle walls were removed. Left ventricles including septum were cut into small pieces of tissue (3 to 5 mm). Explants were placed onto the bottom of 100-mm culture dishes with small amount of culture medium. Explant cultures were left untreated for 4 hours to allow for attachment to bottom of dishes in an incubator at 37°C and 5% CO2. Then complete M199 medium (Gibco) was added containing (mM) NaCl 117, KCl 5.3, $CaCl_2$ 1.8, $MgSO_4$ 0.8, $NaHCO_3$ 26.2, and Na_2HPO_4 1.0, supplemented with 5% fetal bovine serum, 1% penicillin/streptomycin, 5 mg/ml insulin, 5 mg/ml transferrin, 5 ng/ml selenium, and 2 mM L-glutamine. Explant cultures were separated into three groups for treatments: Tg+AngII mice treated with vehicle (saline), 0.5 µM rapamycin or 0.5 µM NF-kB inhibitor pyrrolidine dithiocarbamate (PDTC). The treatment lasted for 24 hours. Explants were harvested and subjected to western blot analyses.

References

1. Ullevig S, Zhao Q, Lee CF, Seok Kim H, Zamora D, Asmis R. NADPH oxidase 4 mediates monocyte priming and accelerated chemotaxis induced by metabolic stress. *Arterioscler Thromb Vasc Biol*. 2012;32:415-26
2. Lee CF, Qiao M, Schröder K, Zhao Q, Asmis R. Nox4 is a novel inducible source of reactive oxygen species in monocytes and macrophages and mediates oxidized low density lipoprotein-induced macrophage death. *Circ Res*. 2010;106:1489-97
3. Maalouf RM, Eid AA, Gorin YC, Block K, Escobar GP, Bailey S, Abboud HE. Nox4-derived reactive oxygen species mediate cardiomyocyte injury in early type 1 diabetes. *Am J Physiol Cell Physiol*. 2012;302:C597-604
4. Guzik TJ, Mussa S, Gastaldi D, Sadowski J, Ratnatunga C, Pillai R, Channon KM. Mechanisms of increased vascular superoxide production in human diabetes mellitus: role of NADPH oxidase and endothelial nitric oxide synthase. *Circulation*. 2002;105:1656-62
5. Velagapudi C, Bhandari BS, Abboud-Werner S, Simone S, Abboud HE, Habib SL. The tuberin/mTOR pathway promotes apoptosis of tubular epithelial cells in diabetes. *J Am Soc Nephrol*. 2011;22:262-73
6. Zhao Q, Ishibashi M, Hiasa K, Tan C, Takeshita A, Egashira K. Essential role of vascular endothelial growth factor in angiotensin II-induced vascular inflammation and remodeling. *Hypertension*. 2004;44:264-70
7. Zhao Q, Egashira K, Inoue S, Usui M, Kitamoto S, Ni W, Ishibashi M, Hiasa Ki K, Ichiki T, Shibuya M, Takeshita A. Vascular endothelial growth factor is necessary in the development of arteriosclerosis by recruiting/activating monocytes in a rat model of long-term inhibition of nitric oxide synthesis. *Circulation*. 2002;105:1110-5

Supplemental Table S1: The systemic cardiac indices of mice

	CTL	Tg	CTL+AngII	Tg+AngII
Sex	Male	Male	Male	Male
Age	19 w ks	19 w ks	19 w ks	19 w ks
Body w eight	28.5 ± 2.1	28 ± 1.9	28.7 ± 2.3	28.3 ± 2.0
Heart w eight	0.119 ± 0.009	0.121± 0.011	0.147± 0.010*	0.161± 0.013#
Heart/body (%)	0.417± 0.034	0.432 ± 0.032	0.511± 0.020*	0.569 ± 0.023#
Mean blood pressure	105 ± 10	106 ± 8	130 ± 15*	135 ± 11#
Heart rate	400 ± 51	418 ± 73	397 ± 60	436 ± 82

Note: Characteristics are measured/recorded at the end of AngII or vehicle infusion. CTL indicates control mice; Tg, cardiac specific human Nox4 transgenic mice; CTL+AngII and Tg+AngII, angiotensin II-infused mice. *$P < 0.05$ *vs* WT or Tg. #$P < 0.01$ *vs* WT or Tg. n = 6.

Supplemental Table S2: List of antibodies used in the immunoblot assays.

Antibody	Cat #	Company	Antibody	Cat #	Company
Nox1	NBP1-31546	Novus	Akt	9272	Cell Signaling
Nox2	070024	Millipore	P-mTOR (S2448)	5536	Cell Signaling
Nox3	sc-67005	Santa Cruz	P-Raptor (S792)	2083	Cell Signaling
Nox4	sc-30141	Santa Cruz	Raptor	2280	Cell Signaling
Nox4	3187-1	Epitomics	P-P70S6 (T389)	9234	Cell Signaling
Fibronectin	2745	Cell Signaling	P70S6	9202	Cell Signaling
TGF-β1	3709	Cell Signaling	P-4EBP1 (T37/46)	2855	Cell Signaling
ANP	sc-20158	Santa Cruz	4EBP1	9644	Cell Signaling
Tropomyosin	sc-74480	Santa Cruz	P-P65 (S536)	3033	Cell Signaling
Myocardin	sc-33766	Santa Cruz	P-P65 (S468)	3039	Cell Signaling
MyH7 (βMHC)	sc-71575	Santa Cruz	P65	8242	Cell Signaling
p-Akt (S473)	9271	Cell Signaling	Gapdh	2118	Cell Signaling
p-Akt (T308)	2965	Cell Signaling			

Supplemental Table S3: List and sequence of primers used in real-time RT-PCR

Gene	Forward primer (5′→3′)	Reverse primer (5′→3′)	PCR product size (bp)	Gene bank number
Nox1	AACATGACAGTGATGTATGCAGC	AACCAAAGCTACAGTGGCAAT	75	NM_172203
Nox2	CCTCTACCAAAACCATTCGGAG	CTGTCCACGTACAATTCGTTCA	119	NM_007807
Nox3	TGGCAGTAAACGCCTATCTGT	CGGAACCCAGAATAACTCGTGTA	90	NM_198958
Mouse Nox4	AAGGTCCCTAGCAGGAGAACA	GCTACATGCACACCTGAGAAA	101	NM_015760
Human Nox4	ACCTTTGTGCCTGTACTGTGCC	TGTTGCTTTGGTTTCAGTTGG AC	232	AB041035.1
TGF-β1	CCACCTGCAAGACCATCGAC	CTGGCGAGCCTTAGTTTGGAC	91	NM_011577
Collagen-1α1	GCTCCTCTTAGGGGCCACT	ATTGGGGACCCTTAGGCCAT	91	NM_007742
Collagen-3α1	CTGTAACATGGAAACTGGGGAAA	CCATAGCTGAACTGAAAACCACC	144	NM_009930
CTGF	GACCCAACTATGATGCGAGCC	CCCATCCCACAGGTCTTAGAAC	77	NM_010217
PAI-1	AGAAACGGGACAAACTTCGTC	GTCTTGCACTGTATAGCCGAG	126	NM_001199945
GAPDH	AGCTTCGGCACATATTTCATCTG	CGTTCACTCCCATGACAAACA	89	NM_008085

Supplemental Table S4: Characteristics of mice treated with vehicle or tamoxifen

	Vehicle (n = 10)			Tamoxifen (n = 6)		
	C57BL/6J	Cre	LSL-hNox4	C57BL/6J	Cre	LSL-hNox4
Age (wks)	19	19	19	19	19	19
Body weight (g)	30 ± 1.7	31± 2.3	30.6 ± 2.0	29.8 ± 3.0	32 ± 2.5	31 ± 2.6
Mean BP (mmHg)	103 ± 8	104 ± 9	106 ± 10	102 ± 11	108 ± 9	109 ± 7
Heart rate	508 ± 23	490 ± 28	510 ± 35	486 ± 20	500 ± 30	503 ± 25
LV weight (mg)	109 ± 6	105 ± 5	110 ± 7	108 ± 4	105 ± 6	109 ± 8
ROS (fold in intensity)	1	1.1 ± 0.2	0.9 ± 0.5	1.2 ± 0.3	0.9 ± 0.3	1.1 ± 0.4
Fibrosis (% of section)	0.6 ± 0.2	0.5 ± 0.3	0.5 ± 0.1	0.6 ± 0.1	0.4 ± 0.3	0.5 ± 0.2
Myocyte size (μm^2)	310 ± 11	296 ± 16	303 ± 10	315 ± 18	301 ± 20	311 ± 21
Dead cells (/section)	ND	ND	ND	ND	ND	ND

treatment

Note: Data shown in the table were recorded after 7 days of vehicle or tamoxifen treatment followed by 14 days of vehicle. ROS production was measured with fluorescent sensor HyPer. Fibrosis is shown as area percentage in one cross-section. ND indicates not detectable.

Supplemental Figure Legends

Supplemental Figure S1: A, The Cre-Lox Technology for targeted homologous recombination of transgene hNox4. B, Timeframe of animal treatments. Mice at age of 16 weeks were treated with tamoxifen at a dose of 1 mg/ml in the drinking water for 7 days. Tamoxifen treatment was stopped and vehicle or Ang II were infused by i.p. Alzet micro-osmotic pumps (Model 1004) filled with angiotensin II at a concentration of 1 µg/kg/min for 14 days. For GKT treated group, GKT137831 treatment started at the same time as tamoxifen in the drinking water and lasted 3 weeks. Mice were sacrificed and tissues were harvested at the end of AngII infusion. C. RT-PCR blotting confirming specificity of primers used for detecting human (hNox4) or mouse Nox4 RNA (mNox4). There is no cross-reaction between the species. Lane M: a 100-bp ladder. Lane 1: Mouse heart RNA with mouse Nox4 primers; Lane 2: Mouse heart RNA with human Nox4 primers; Lane 3: Human cardiomyocytes RNA with mouse Nox4 primers; Lane 4: Human cardiomyocytes RNA with human Nox4 primers; Lane 5: mouse heart RNA with actin primers; Lane 6: Human cardiomyocytes RNA with actin primers.

Supplemental Figure S2: Radial distribution of 16 fields of a cross-section of LV wall chosen for quantitative morphometrics. Each of 8 radial lines from the center of the LV lumen has two circles depicting the loci where images at 400× magnification were captured under a microscope Zeiss Fluorescent Axio Scope-A1 with AxioCam MRc5 camera. LV tissue was cut into three parts, apex, middle and bottom, horizontally. 3 serial cross-cryosections of the middle part at a 300-µm-interval were used for morphological analyses including quantification of fibrotic area, evaluation of cardiac myocyte size, evaluation of DHE stain intensity, alpha-SM-actin positive fibroblast area, apoptotic cell counting. Total 48 images (views) were captured for one LV.

Supplemental Figure S3. ROS levels induced by overexpression of hNox4 transgene and or angiotensin II. Upper panel: Representative microphotographs of LV tissue with DHE staining. Frozen sections of LV tissue were stained with DHE. The density of red fluorescence reflects intracellular concentration of super oxide. See detail protocol in Methods. The bar figure shows quantification of fluorescent intensity. *P < 0.01 vs the rest groups. #P < 0.01 vs the Tg or CTL+AngII. No significant difference between Tg and CTL+AngII. n = 6.

Supplemental Figure S4. Nox4 overexpression and angiotensin II induce myocardial apoptosis. A, Representative microphotographs showing apoptotic cardiomyocytes (bright green dots) recognized by Tunnel fluorescent staining counterstained with DAPI for nuclei. B, Data are shown as M±SD of apoptotic cells/section, summarized from 48 views of 3 serial cross-sections at 300 µm interval of LV at the level of the papillary muscles. GKT137831 inhibition of Nox4 protects myocardium from apoptosis. *P < 0.01 vs the rest groups except Tg+AngII+GKT. #P < 0.01 vs the rest groups.

Supplemental Figure S5. Proliferation/differentiation of fibroblasts and the progression of fibrosis in the LV of Tg+AngII mice. A - C, Representative microphotographs of LV tissue with Masson Trichrome staining. Collagens are stained in blue, muscles in red, and nuclei in black. Purple arrows indicate fibroblasts in earlier stage of differentiation. Fibroblasts in the earlier stage of differentiation are morphologically characterized by a larger elliptical nucleus and appear to secrete small amounts of collagens. Purple arrowheads indicate fibroblasts in later stage of differentiation spindle-shaped with a smaller condensed nucleus and surrounded by more highly dense collagens. White arrows indicate dying myocytes, shrunken and condensed and surrounded by active fibroblasts and initial fibrosis. C, A representative microphotograph

shows fibrosis around a small branch of a coronary artery (ca). D, A representative microphotograph shows cardiac interstitial fibroblasts positively stained with alpha-SM-actin in red fluorescence and nuclei stained in blue fluorescence by DAPI.

Supplemental Figure S6. Proliferation/differentiation of cardiac fibroblasts in LV. A, The representative microphotographs showing cardiac fibroblasts which were recognized by immunofluorescent staining with antibody against α-SM-actin. Fibroblasts are stained in red counterstained with DAPI for nuclei. B, Data are shown as M±SEM of α-SM-actin positive staining area/section (%), summarized from 48 views of 3 serial cross-sections at 300 μm interval of LV at the level of the papillary muscles. C, This diagram explains potential mechanism for the development of cardiac fibrosis. The differentiation/proliferation of cardiac fibroblasts very likely is attributed ROS injury that results in death of cardiac myocytes, leading to paracrine/autocrine increment of cytokines or growth factors to trigger fibroblast proliferation/differentiation. GKT 137831 attenuates fibrotic response by inhibiting Nox4 activity. *P < 0.01 vs the rest groups except Tg+AngII+GKT. #P < 0.01 vs the rest groups.

Supplemental Figure S7. A, Inhibition of Nox4 reduces ROS production induced by overexpression of hNox4 transgene and angiotensin II. Upper panels: Representative microphotographs of LV tissue with DHE staining. Unfixed frozen sections of LV tissue were stained with DHE. The intensity of red fluorescence reflects intracellular concentration of super oxide. See detail protocol in Methods. The bar figure shows quantification of fluorescent intensity, $P < 0.01$ between the two groups. B, H_2O_2 production measured with fluorescent sensor HyPer (Cat #FP941, Evrogen). C. Nox activity measured by the lucigenin-enhanced chemiluminescence method in the LV. D, GKT137831 did not significantly alter expression of cardiac remodeling markers in control mice. *P < 0.01 vs the other groups except of CTL+AngII. #P < 0.01 vs the other groups except of Tg.

Supplemental Figure S8. Pharmacological inhibition of mTOR or NFκB suppresses expression of markers of cardiac remodeling. LV tissues from hNox4 Tg mice infused with AngII were cultured and treated with0.5 μM rapamycin (Rapa) or 0.5 μM PDTC for 24 hours (see detail in Supplemental Methods). Protein expression was analyzed by western blot assay. A, Representative immunoblot showing protein expressions of FN, TGF-β, tropomyosin, myocardin, myH7 and GAPDH in cultured LV tissue. B - F, Quantitative densitometric analyses of the immunoblot data. *$P < 0.001$ vs vehicle. No significant difference in MyH7. n = 5.

Supplemental Figure S9. Comparison of the LV explants cultured for 24 hrs and fresh LV tissue explants. Hematoxylin-eosin (H-E) stain, the TUNEL assay and immunoblot were performed to examine cardiac morphology, cell apoptosis (in bright green fluorescence) and Nox4 expression (in red fluorescence), respectively. The numbers in the panels labeled as Dead Cells indicate the means of apoptotic cells per tissue section in each group. The culture protocol did not significantly increase the number of apoptotic cardiomyocytes in cardiac tissue explants, and Nox4 expression in cultured cardiac explants from Tg mice was similar to that in fresh cardiac tissue explants of the Tg mice. Three mice were used each group.

Supplemental Figure S10. P22phox participates in angiotensin II (AngII) upregulation of Nox4 activity in the LV. A. The qPCR analysis revealed that AngII increases p22phox mRNA expression in the LV. B. Immuno-precipitation followed by immunoblotting revealed that p22phox-Nox4 complex is also increased in the left ventricles of angiotensinII-infused mice compared to control mice. *P < 0.01 vs CTL in panels A to E. *P < 0.01 vs CTL.

Supplemental Figure S11. Subcellular localization of Nox4 Expression of Nox4 protein was quantified in subcellular fractions including endoplasmic reticulum (ER), mitochondria (Mito) and nuclei (Nuc) from the LV tissues of control (CTL) and c-hNox4Tg mice using tissue/cell fractionation and immunoblot protocols (#ab149409 from Abcam, #37612 from Qiagen, and #10088K from Imgenex). The results revealed that Nox4 exists in intracellular fractions at different levels ER > Mito > Nuc, and the transgenic mice express a higher level of Nox4 in each fraction than control mice. pAMPKb1, lamin A/C and cytochrome C are the markers used for ER, nucleus and mitochondria, respectively.

Supplemental Figure S12. Quantification of myocyte size and ratio of reparative fibrosis versus perivascular fibrosis in the LV. A, Representative images of the LV cross-sections from the indicated mice stained with hemotoxylin-eosin (H-E). B, Representative images of the LV cross-sections stained from the indicated mice with wheat germ agglutinin (WGA). The positive staining of WGA is in green. Area of each cardiomyocyte was measured based on the WGA staining and the means are shown in panel C. D, the ratio of reparative fibrosis versus perivascular fibrosis in the LV. The reparative fibrosis defines the interstitial fibrotic area of the LV cross-sections except for the perivascular area. See details for the morphometrics in Online Supplemental Methods.

Supplemental Figure S13. Nox4 expression and fibrosis in the left ventricles of a second line of cardiac specific Nox4 transgenic mice. A, Protein expression of Nox4 measured with Western blot assay. B, Quantification of data of panel A. C. Representative microphotographs showing cardiac fibrosis examined with Masson's Trichrome Staining (blue). D. Quantification of fibrosis shown in panel C. *$P < 0.01$, transgenic (Tg) mice versus control (CTL).

Supplemental Figure S14. Model of Nox4 mediating cardiac remodeling. Excess Nox4 locally in the heart causes cardiac oxidative stress leading to cardiac remodeling, which is associated with activation of the Akt-mTOR and NFkB signaling pathways and reactivation of cardiac fetal contractile genes. Inhibition of Nox4 oxidase blocks the activation of these signaling pathways as well as fetal cardiac genes thereby attenuating cardiac remodeling. Cardiac remodeling is a chronic pathological process induced by accumulated oxidative stress and upregulation of Nox4 resulting in cardiac remodeling. GKT137831 has therapeutic potential to prevent/treat cardiac remodeling and potentially heart failure by blocking Nox4.

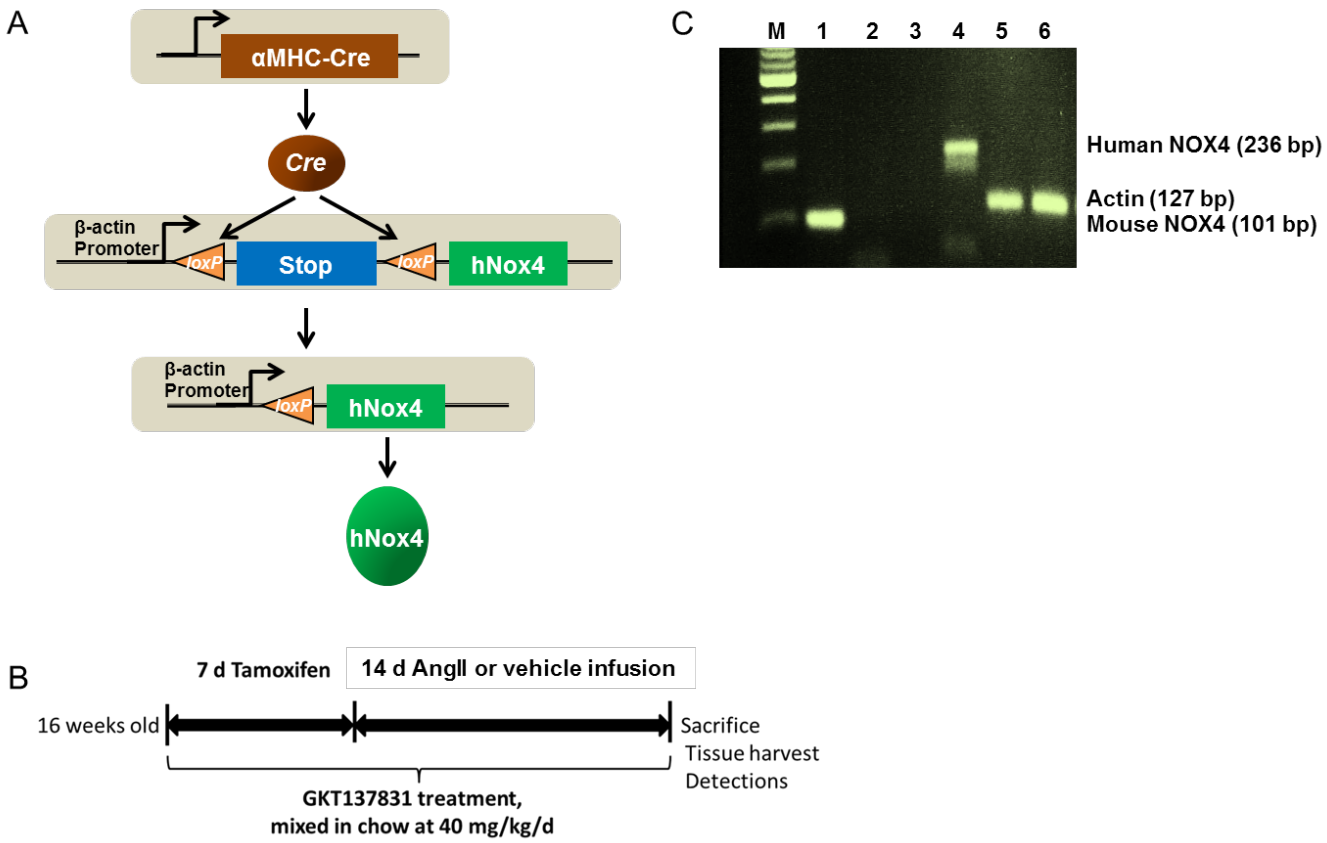

Supplemental Figure S1: A, The Cre-Lox Technology for targeted Homologous recombination of transgene hNox4. B, Timeframe of animal treatments. Mice at age of 16 weeks were treated with tamoxifen at a dose of 1 mg/ml in drinking water for 7 days. Then stop tamoxifen treatment and start Ang II infusion by i.p. Alzet micro-osmotic pumps (Model 1004) fulfilled with angiotensin II at a concentration of 1 µg/kg/min for 14 days. For GKT treated group, GKT137831 treatment started at the same time of tamoxifen drinking and lasted 3 weeks. Mice were sacrificed and tissues were harvested at the end of AngII infusion. C. RT-PCR showing specificity of primers used for detecting human or mouse Nox4 RNA (mNox4 and hNox4). There is no cross-reaction between the species. Lane M: a 100-bp ladder. Lane 1: Mouse heart RNA with mouse Nox4 primers; Lane 2: Mouse heart RNA with human Nox4 primers; Lane 3: Human cardiomyocytes RNA with mouse Nox4 primers; Lane 4: Human cardiomyocytes RNA with human Nox4 primers; Lane 5: mouse heart RNA with actin primers; Lane 6: Human cardiomyocytes RNA with actin primers.

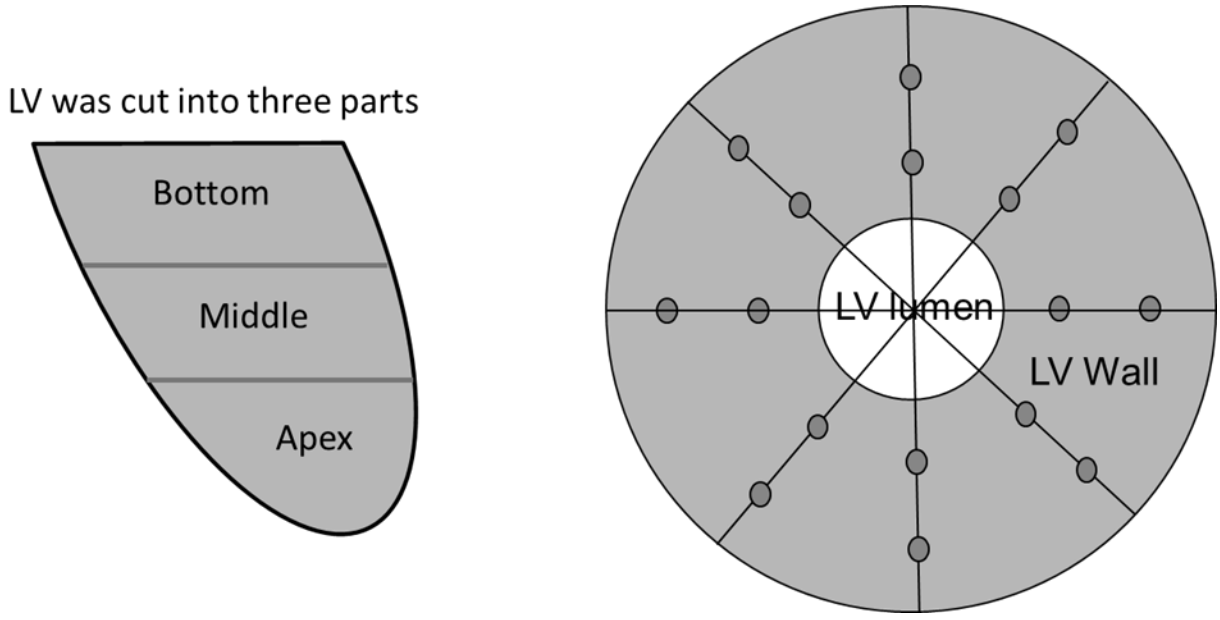

Supplemental Figure S2: Radial distribution of 16 fields of a cross-section of LV wall chosen for quantitative morphometrics. Each of 8 radial lines from the center of the LV lumen has two circles depicting the loci where images at 400× magnification were captured under a microscope Zeiss Fluorescent Axio Scope-A1 with AxioCam MRc5 camera. LV tissue was cut into three parts, apex, middle and bottom, horizontally. 3 serial cross-cryosections of the middle part at a 300-µm-interval were used for morphological analyses including quantification of fibrotic area, evaluation of cardiac myocyte size, evaluation of DHE stain intensity, alpha-SM-actin positive fibroblast area, apoptotic cell counting. Total 48 images (views) were captured for one LV.

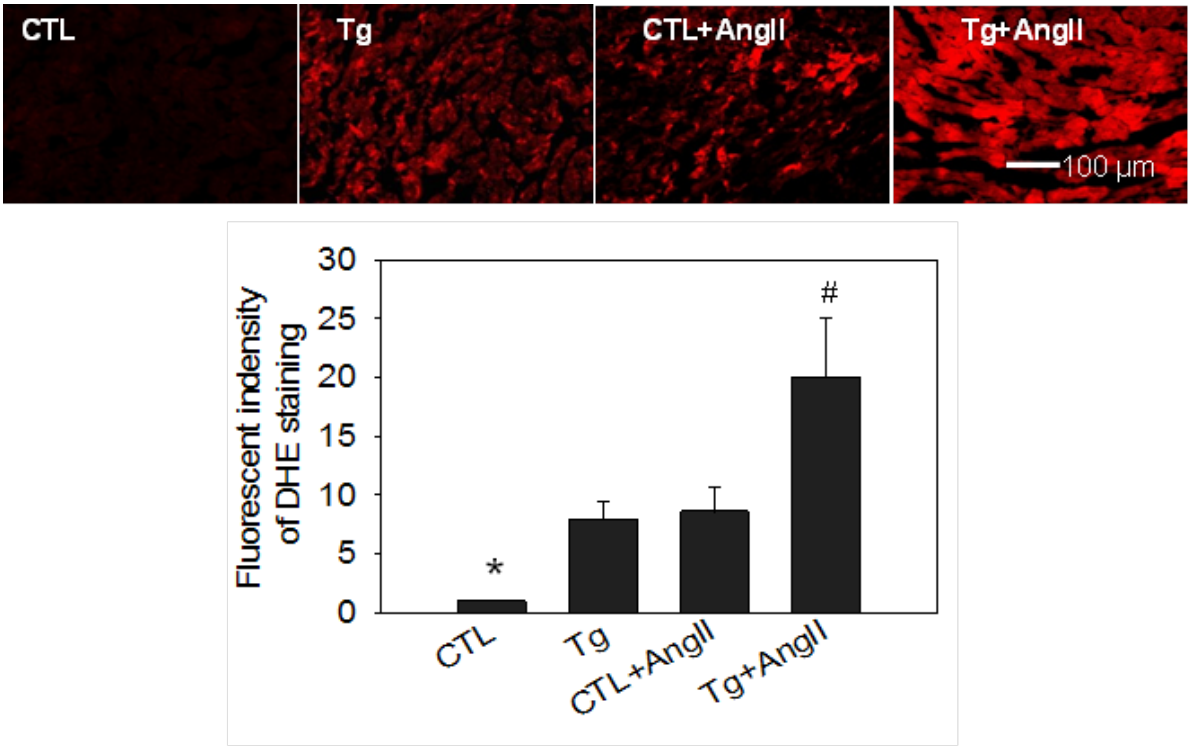

Supplemental Figure S3. ROS levels induced by overexpression of hNox4 transgene and or angiotensin II. Upper panel: Representative microphotographs of LV tissue with DHE staining. Frozen sections of LV tissue were stained with DHE. The density of red fluorescence reflects intracellular concentration of super oxide. See detail protocol in Methods. The bar figure shows quantification of fluorescent intensity. *P < 0.01 vs the rest groups. #P < 0.01 vs the Tg or CTL+AngII. No significant difference between Tg and CTL+AngII. n = 6.

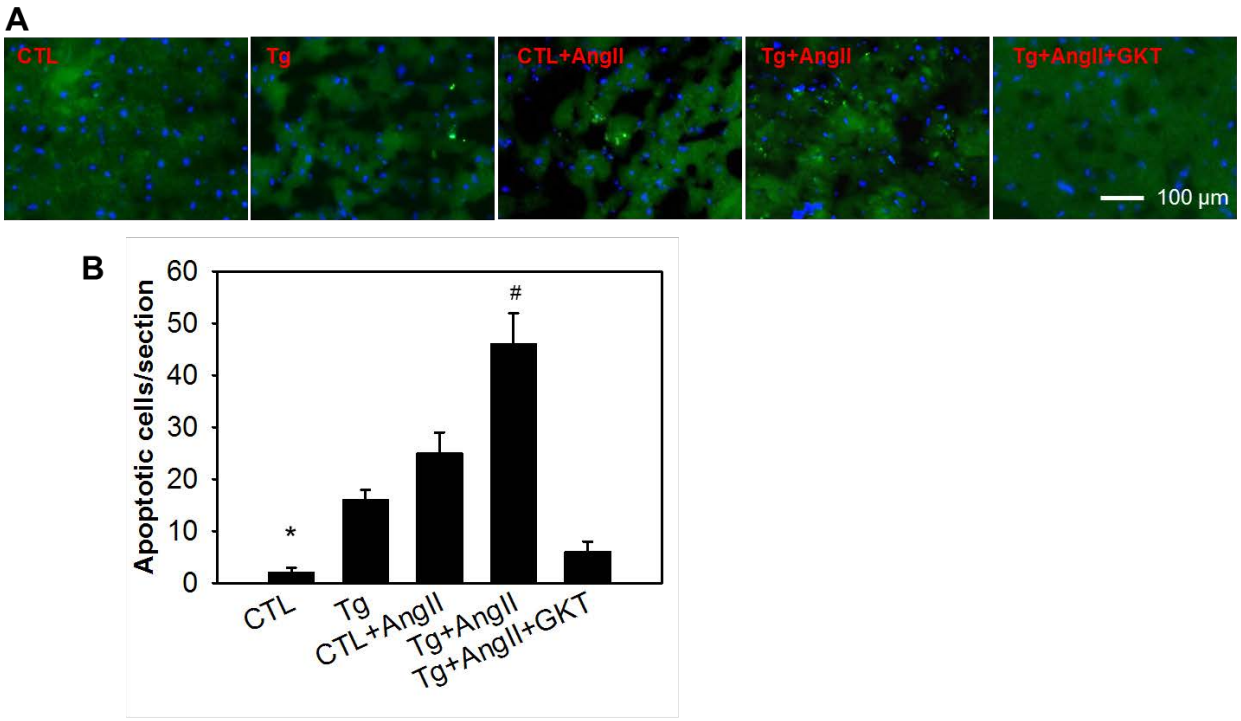

Supplemental Figure S4. Nox4 overexpression and angiotensin II induce myocardial apoptosis. A, Representative microphotographs showing apoptotic cardiomyocytes (bright green dots) recognized by Tunnel fluorescent staining counterstained with DAPI for nuclei. B, Data are shown as M±SD of apoptotic cells/section, summarized from 48 views of 3 serial cross-sections at 300 μm interval of LV at the level of the papillary muscles. GKT137831 inhibition of Nox4 protects myocardium from apoptosis. *P < 0.01 vs the rest groups except Tg+AngII+GKT. #P < 0.01 vs the rest groups.

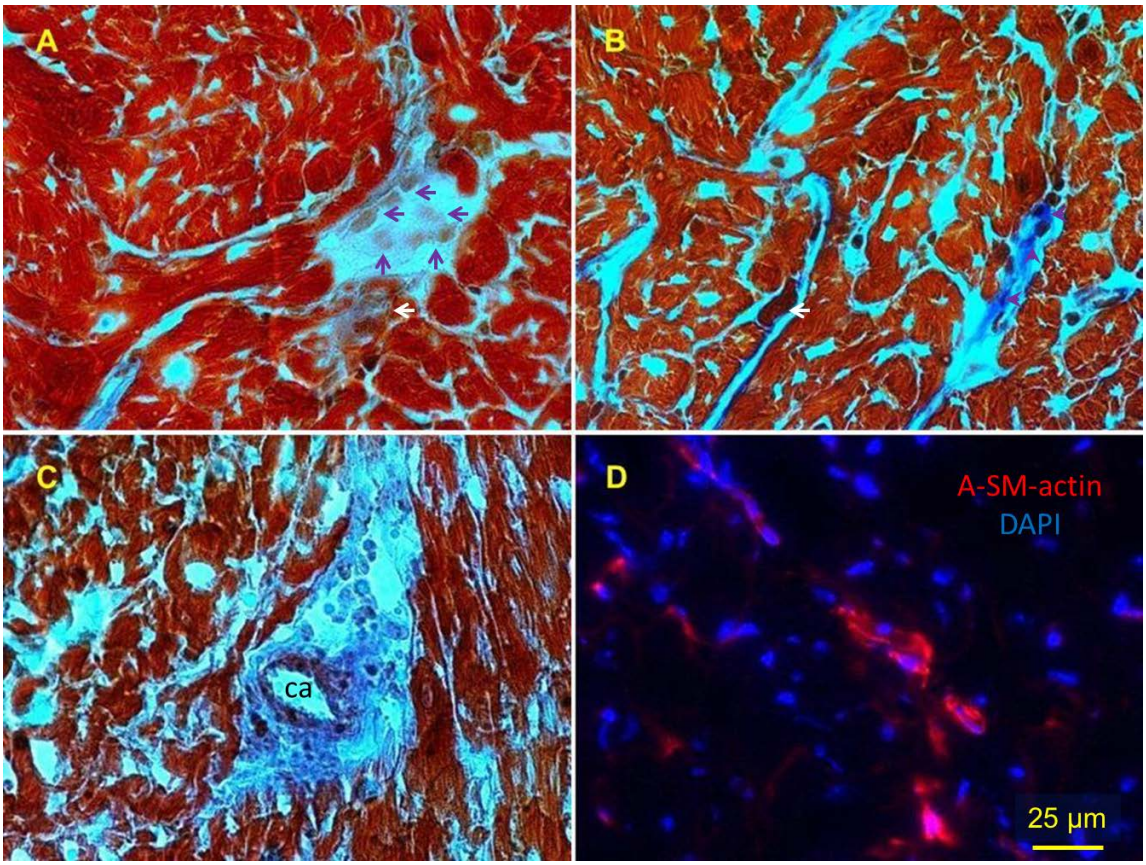

Supplemental Figure S5. Proliferation/differentiation of fibroblasts and the progression of fibrosis in the LV of Tg+AngII mice. A - C, Representative microphotographs of LV tissue with Masson Trichrome staining. Collagens are stained in blue, muscles in red, and nuclei in black. Purple arrows indicate fibroblasts in earlier stage of differentiation. Fibroblasts in the earlier stage of differentiation are morphologically characterized by a larger elliptical nucleus and start to secrete small amounts of collagens. Purple arrowheads indicate fibroblasts in later stage of differentiation spindle-shaped with a smaller condensed nucleus and surrounded by more highly dense collagens. White arrows indicate dying myocytes, shrunken and condensed and surrounded by active fibroblasts and interstitial fibrosis. C, A representative microphotograph shows fibrosis around a small branch of a coronary artery (ca). D, A representative microphotograph shows cardiac interstitial fibroblasts positively stained with alpha-SM-actin in red fluorescence and nuclei stained in blue fluorescence by DAPI.

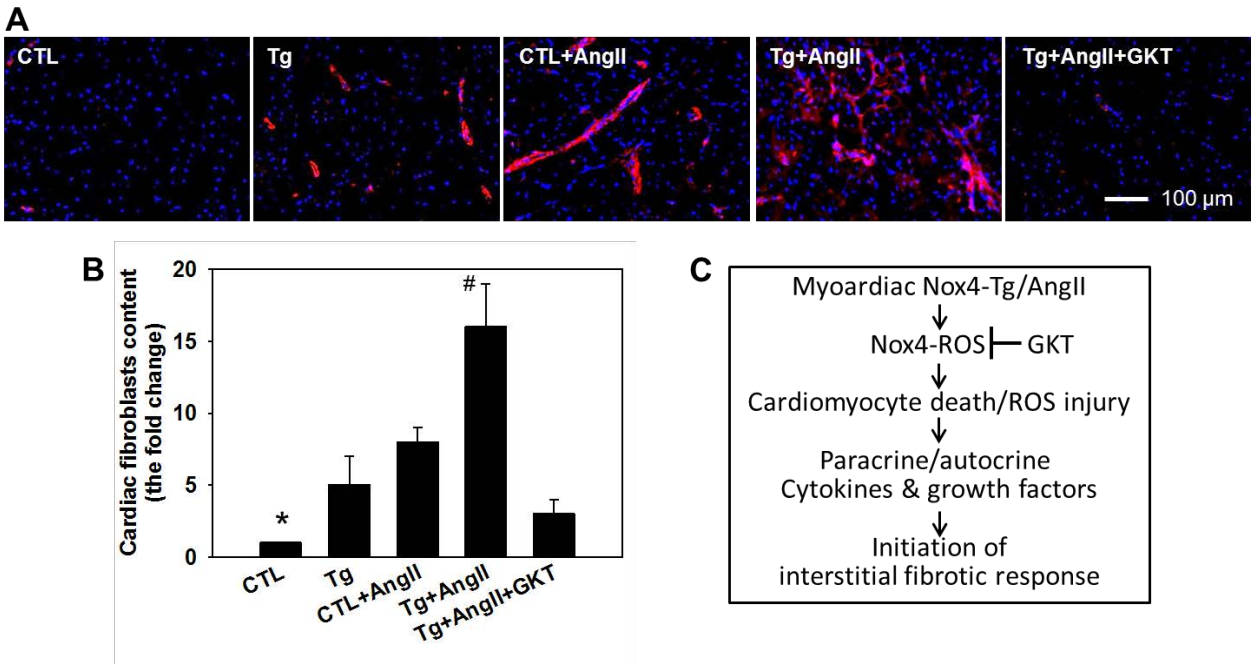

Supplemental Figure S6. Proliferation/differentiation of cardiac fibroblasts in the LV. A, Representative microphotographs showing cardiac fibroblasts which were recognized by immunofluorescent staining with antibody against α-SM-actin. Fibroblasts are stained in red counterstained with DAPI for nuclei. B, Data are shown as M±SEM of α-SM-actin positive staining area/section (%), summarized from 48 views of 3 serial cross-sections at 300 μm interval of LV at the level of the papillary muscles. C, This diagram depicts potential mechanism for the development of cardiac fibrosis. The differentiation/proliferation of cardiac fibroblasts very likely is attributed to Nox4 upregulation-mediated ROS injury that results in death of cardiac myocytes, leading to paracrine/autocrine increment of cytokines or growth factors to trigger fibroblast proliferation/differentiation. GKT 137831 attenuates fibrotic response by inhibiting Nox4 activity. *P < 0.01 vs the rest groups except Tg+AngII+GKT. #P < 0.01 vs the rest groups.

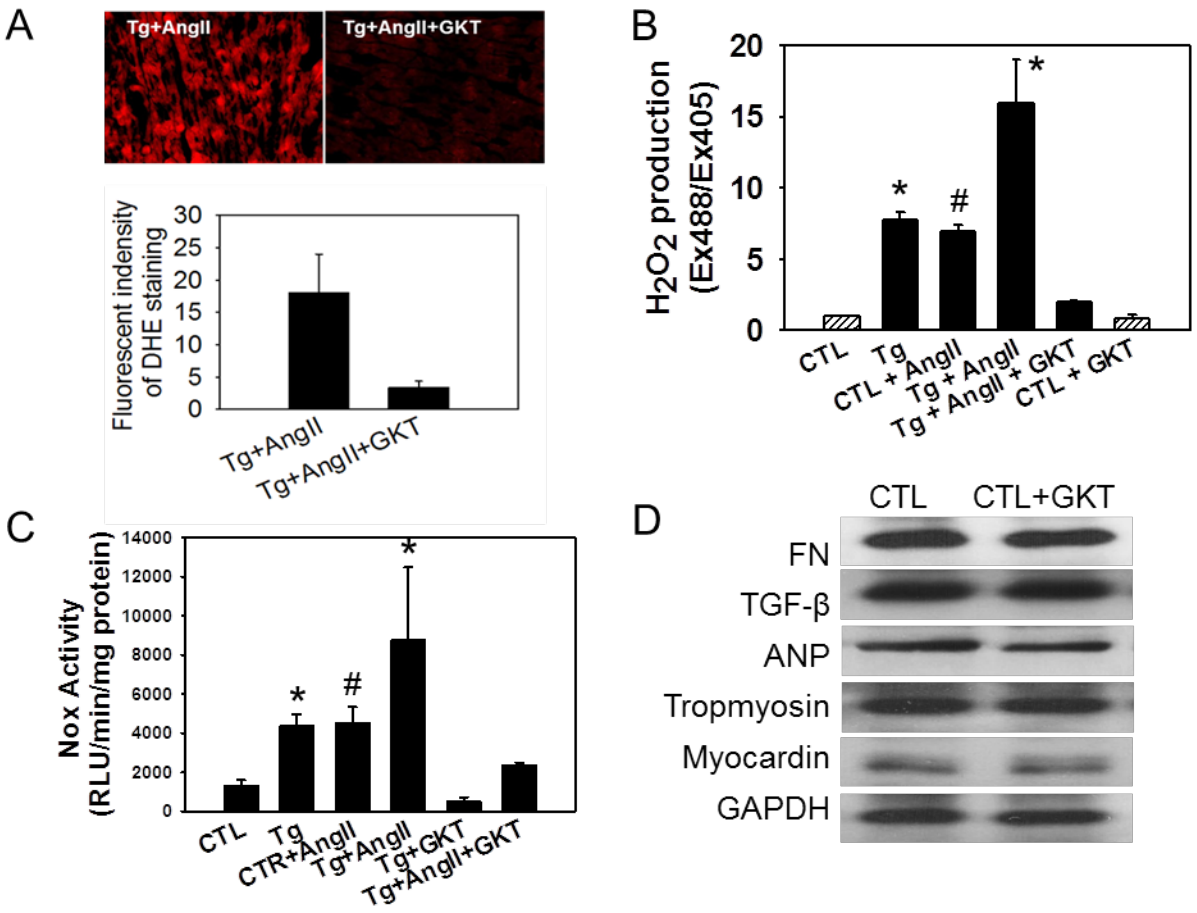

Supplemental Figure S7. A, Inhibition of Nox4 reduces ROS production induced by overexpression of hNox4 transgene and angiotensin II. Upper panels: Representative microphotographs of LV tissue with DHE staining. Unfixed frozen sections of LV tissue were stained with DHE. The intensity of red fluorescence reflects intracellular concentration of super oxide. See detail protocol in Methods. The bar figure shows quantification of fluorescent intensity, $P < 0.01$ between the two groups. B, H_2O_2 production measured with fluorescent sensor HyPer (Cat #FP941, Evrogen). C. Nox activity measured by the lucigenin-enhanced chemiluminescence method in the LV. D, GKT137831 did not significantly alter expression of cardiac remodeling markers in control mice. *P < 0.01 vs the other groups except of CTL+AngII. #P < 0.01 vs the other groups except of Tg.

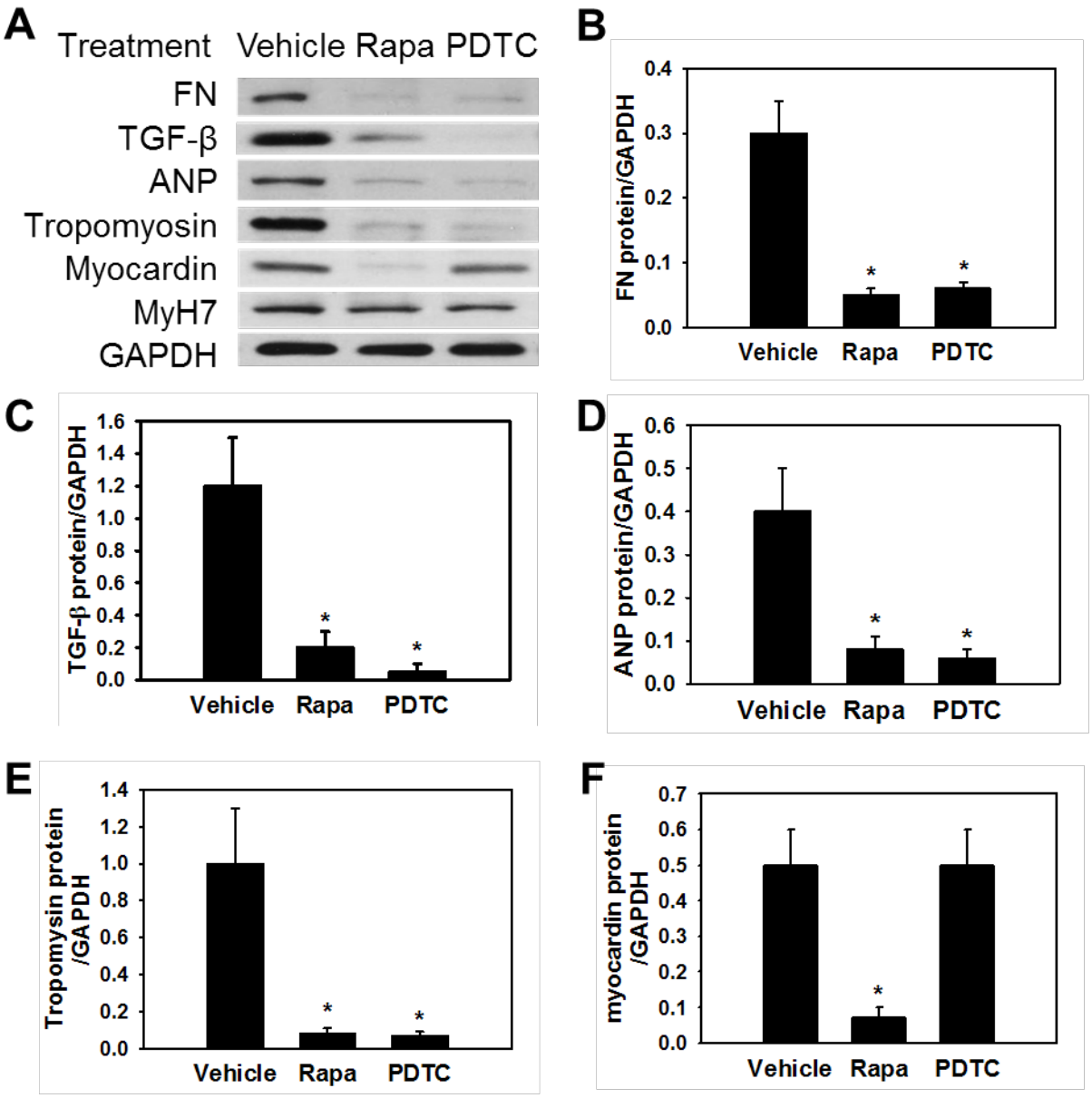

Supplemental Figure S8. Pharmacological inhibition of mTOR or NFκB suppresses expression of markers of cardiac remodeling. LV tissues from hNox4 Tg mice infused with AngII were cultured and treated with0.5 μM rapamycin (Rapa) or 0.5 μM PDTC for 24 hours (see detail in Supplemental Methods). Protein expression was analyzed by western blotting. A, Representative immunoblot showing protein expression of FN, TGF-β, tropomyosin, myocardin, myH7 and GAPDH in cultured LV tissue. B - F, Quantitative densitometric analyses of the immunoblot data. *$P < 0.001$ vs vehicle. No significant difference in MyH7. n = 5.

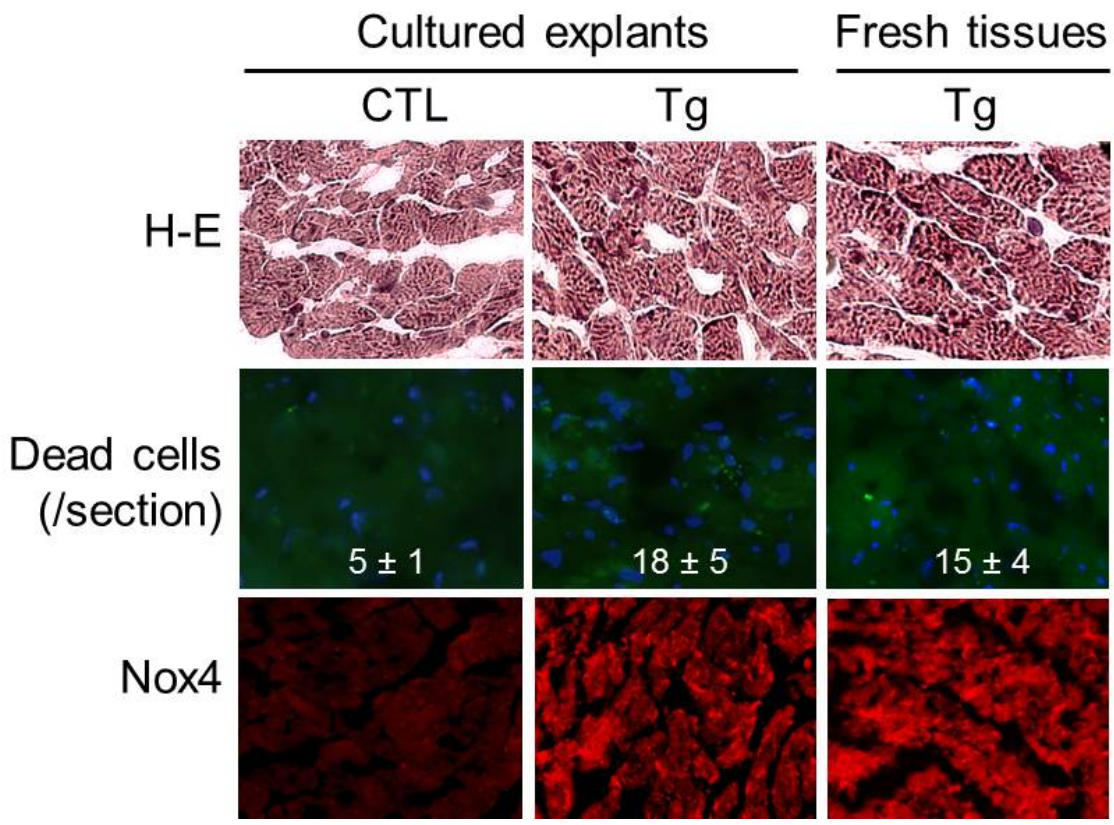

Supplemental Figure S9. Comparison of the LV explants cultured for 24 hrs and fresh LV tissue explants. Hematoxylin-eosin (H-E) stain, TUNEL assay and immunofluorescence were performed to examine cardiac morphology, cell apoptosis (in bright green fluorescence) and Nox4 expression (in red fluorescence). The numbers in the panels labeled as Dead Cells indicate the means of apoptotic cells per tissue section in each group. The culture protocol did not significantly increase cardiomyocyte death in the explants, and Nox4 expression in cultured cardiac explants from Tg mice was similar to that in fresh cardiac tissues of Tg mice. Three mice were used each group.

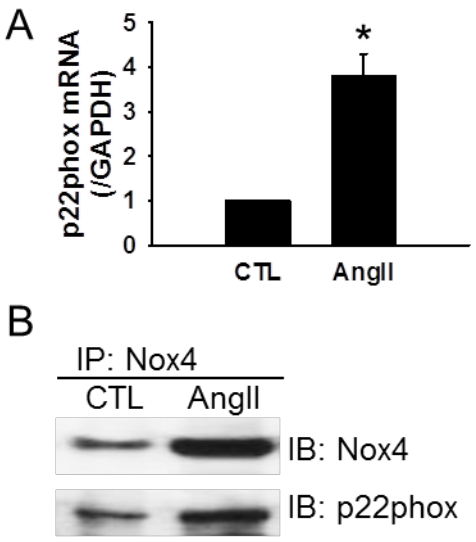

Supplemental Figure S10. P22phox participates in angiotensin II (AngII) upregulation of Nox4 activity in the LV. A. The qPCR analysis revealed that AngII increases p22phox mRNA expression in the LV. B. Immuno-precipitation followed by immunoblotting revealed that p22phox-Nox4 complex is also increased in the left ventricles of angiotensinII-infused mice compared to control mice. *P < 0.01 vs CTL in panels A to E. *P < 0.01 vs CTL.

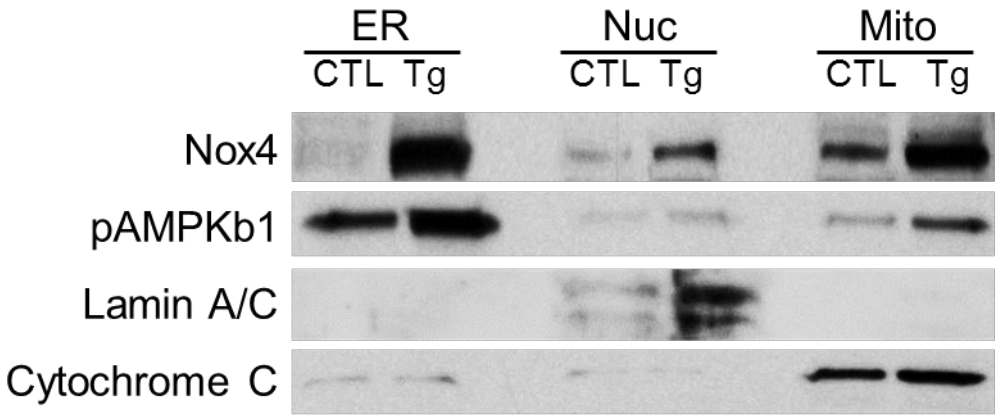

Supplemental Figure S11. Subcellular localization of Nox4. Nox4 expression was quantified in subcellular fractions including endoplasmic reticulum (ER), mitochondria (Mito) and nuclei (Nuc) from the LV tissue of control (CTL) and c-hNox4Tg mice using tissue/cell fractionation and immunoblot protocols (#ab149409 from Abcam, #37612 from Qiagen, and #10088K from Imgenex). The results revealed that Nox4 exists in intracellular fractions, but with different levels of expression ER > Mito > Nuc, and the transgenic mice exhibit a higher level of Nox4 in each fraction than control mice. pAMPKb1, lamin A/C and cytochrome C are the markers used for ER, nucleus and mitochondria, respectively.

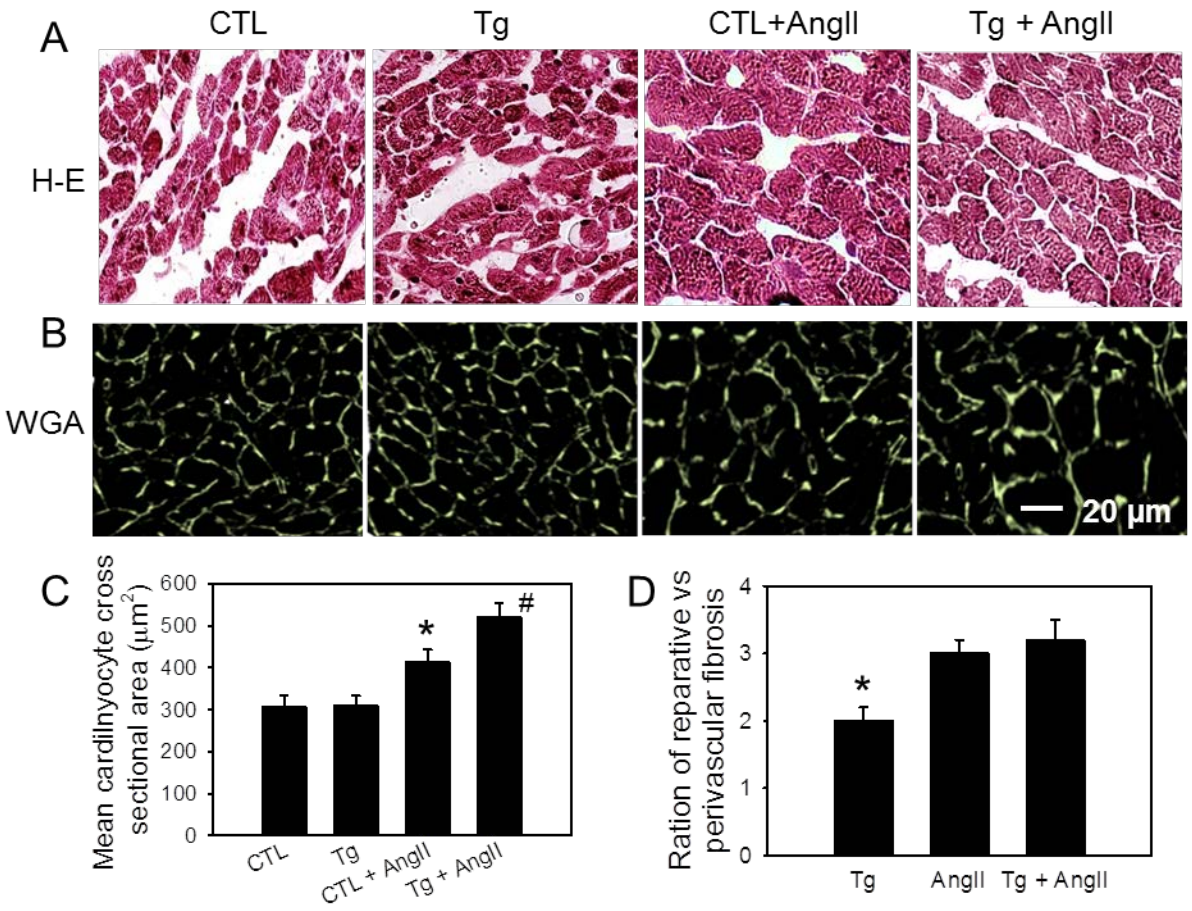

Supplemental Figure S12. Quantification of myocyte size and ratio of reparative fibrosis versus perivascular fibrosis in the LV. A, Representative images of the LV cross-sections from the indicated mice stained with hemotoxylin-eosin (H-E). This is a color version of Figure 4A. B, Representative images of the LV cross-sections stained from the indicated mice with wheat germ agglutinin (WGA). The positive staining of WGA is in green. Area of each cardiomyocyte was measured based on the WGA staining and the means are shown in panel C. D, the ratio of reparative fibrosis versus perivascular fibrosis in the LV. The reparative fibrosis defines the interstitial fibrotic area of the LV cross-sections except of the perivascular area. See the details for the morphometrics in Online Supplemental Methods.

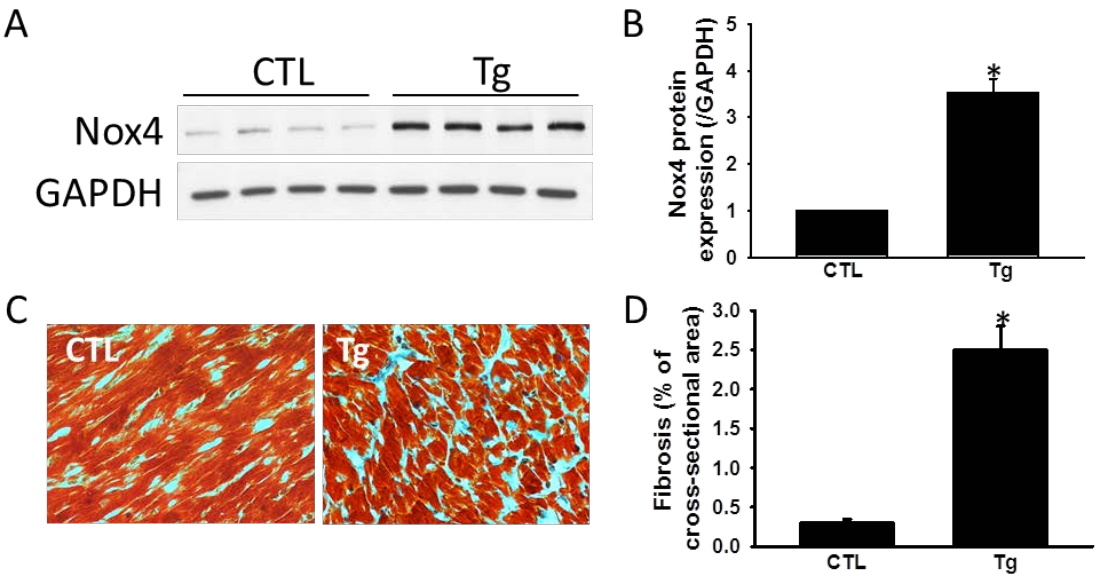

Supplemental Figure S13. Nox4 expression and fibrosis in the left ventricles of a second line of cardiac specific Nox4 transgenic mice. A, Protein expression of Nox4 measured with Western blot assay. B, Quantification of data of panel A. C. Representative microphotographs showing cardiac fibrosis examined with Masson's Trichrome Staining (blue). D. Quantification of fibrosis shown in panel C. *P < 0.01, transgenic (Tg) mice versus control (CTL).

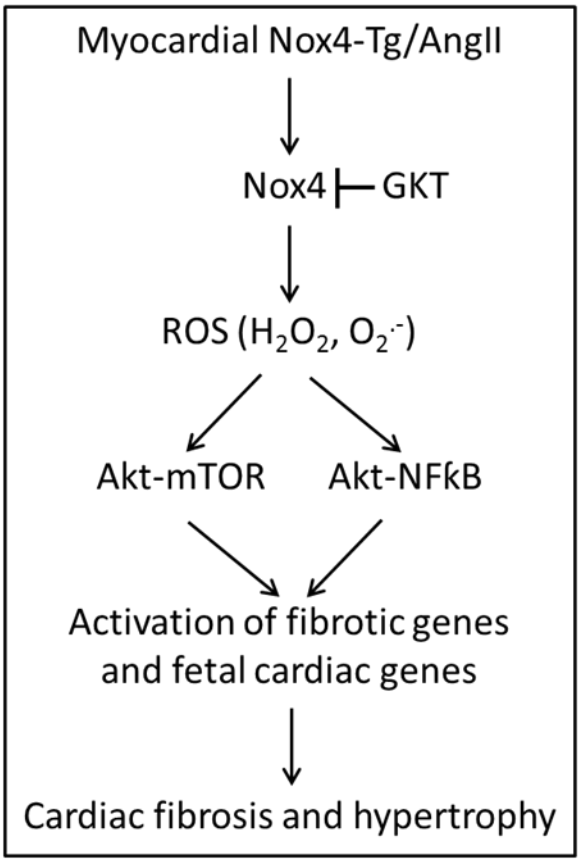

Supplemental Figure S14. Model of Nox4 mediating cardiac remodeling. Excess Nox4 locally in the heart causes cardiac oxidative stress leading to cardiac remodeling, which is associated with activation of the Akt-mTOR and NFκB signaling pathways and revival of cardiac fetal contractile genes. Inhibition of Nox4 oxidase blocks the activation of these signaling pathways and revival of the fetal cardiac genes thereby attenuating cardiac remodeling. Cardiac remodeling is a chronic pathological process induced by accumulated oxidative stress. Even upregulation of Nox4 alone could result in cardiac remodeling when the upregulation in the heart reaches an enough high level by forced overexpression technologies or pharmacological stimuli. GKT137831 has therapeutic potential to prevent/treat cardiac remodeling and potentially heart failure by blocking Nox4 upregulation.